

Barrier Layers in a High-resolution Model in the Eastern Tropical Pacific

F. M. Bingham¹, Z. Li², S. Katsura³, J. Sprintall³

¹University of North Carolina Wilmington, Center for Marine Science, Wilmington, NC, USA.

²California Institute of Technology, Jet Propulsion Laboratory, Pasadena, CA, USA.

³Scripps Institution of Oceanography, University of California, San Diego

Corresponding author: Frederick M. Bingham (binghamf@uncw.edu)

Key Points:

- Salinity barrier layers (BLs) in the eastern tropical North Pacific are characterized using a high-resolution numerical model
- BLs are associated with surface salinity fronts which tilt towards the fresh side at their base
- Vertical circulation combined with surface divergence and convergence are proposed as another formation mechanism for BLs in this region.

18 **Abstract**

19 This study examines salinity barrier layers (BLs) in the eastern tropical North Pacific (ETP) in
20 the region of the SPURS-2 (Salinity Processes in the Upper ocean Regional Studies – 2) field
21 campaign. We utilize a high-resolution numerical model to study BLs and their relationship to
22 frontal features and small-scale ocean variability, focusing on two specific events. One is
23 associated with a large outbreak of BL presence near 7°N along 125°W. The other is a relatively
24 isolated but persistent BL that forms near 13°N, again along 125°W. In both cases we find that
25 the BL is proximate to a salinity frontal feature in which isohalines tilt toward the fresh side of
26 the front at its base. The BLs studied are associated with divergent flow at the surface on the
27 fresh side of the front and convergent flow on the salty side. Tilting of the front is invoked to
28 explain this, with an additional mechanism involving a vertical circulation which causes the base
29 of the front to tilt preferentially.

30 **Plain Language Summary**

31 Salinity barrier layers (BLs) are common in the eastern tropical North Pacific (ETP) ocean. They
32 consist of a surface mixed layer that is homogeneous in temperature, but with a high salinity
33 layer at the base. They may play an important role in regulating the transfer of heat, momentum
34 and freshwater across the ocean surface and from there into the interior. This study examines
35 BLs in the ETP in the region of the SPURS-2 (Salinity Processes in the Upper ocean Regional
36 Studies – 2) field campaign using a high-resolution numerical simulation. SPURS-2 took place in
37 2016-2017 and was designed to study processes connecting salinity and rainfall in the ETP in the
38 vicinity of the intertropical convergence zone. Two specific examples of BLs are studied. In one,
39 there is a large outbreak of such layers throughout the ETP along a large-scale sea surface
40 salinity (SSS) front. In the other example, the BL was an isolated feature associated with another
41 sharp SSS front. So frontal features are an important part of the process of BL formation. In
42 addition, we find surface flow which converges towards the front on the salty side and diverges
43 away from it on the fresh side. BL formation at the front is a result of the front tilting away from
44 the vertical, and in the case of the fronts studied here, that tilting is concentrated at the front's
45 base. It is also likely associated with vertical circulation on either side of it.

46

47 **1 Introduction**

48 Barrier layers (BLs) are areas in the upper ocean where the surface mixed layer as
49 defined by temperature is greater than that as defined by density due to the presence of salty
50 water at the base of the mixed layer. They have been observed in the ocean since their discovery
51 about 30 years ago (Godfrey and Lindstrom, 1989; Lukas and Lindstrom, 1991). BLs have been
52 found in a diverse set of contexts (Sprintall and Tomczak, 1992; de Boyer Montegut et al., 2007),
53 most especially in the tropics and at high latitudes, and are an important part of upper ocean
54 dynamics in these areas (Roemmich et al., 1994; Vialard and Delecluse, 1998a). In the tropics in
55 particular, they are thought to modulate air-sea interaction by creating a layer of insulating
56 stratification, which can magnify the impact of heat and/or freshwater flux at the surface (Maes
57 et al., 2002; Maes et al., 2005). They also act to suppress entrainment cooling at the base of the
58 mixed layer, since water in the mixed layer is at the same temperature as water below it (Godfrey
59 and Lindstrom, 1989; Vialard and Delecluse, 1998b).

60 BLs have been extensively studied in the western Pacific, but not as much in the eastern
61 Pacific. Conditions are different in the eastern part of the basin where the forcing is more
62 seasonal. Katsura and Sprintall (2020; henceforth “KS20”) have shown that BLs are ubiquitous
63 in the eastern tropical Pacific (ETP) under the intertropical convergence zone (ITCZ) (Qu et al.,
64 2014). Their presence is highly seasonal, with maximum likelihood and thickness in the summer
65 and fall (de Boyer Montegut et al., 2007). The KS20 study was a climatological seasonal one
66 based on sparse Argo data, so BLs were only discussed on a monthly time scale. KS20 attribute
67 the common presence of BLs in this region to convergent Ekman transport driven by wind stress
68 curl. The Ekman convergence creates mixed layer salinity fronts, which then tilt due to
69 instability and shear between the surface and the base of the mixed layer. This process of tilting
70 was first proposed by Cronin and McPhaden (2002; henceforth “CM02”) as one potential
71 mechanism for BL formation. KS20’s conclusion is congruent with Sato et al., (2004), Sato et al.
72 (2006), and Katsura et al. (2015), who all emphasized the role of sharp small-scale salinity fronts
73 and subduction of high salinity water in the tropical and subtropical ocean. However, the
74 conclusions of KS20 and those of Sato et al. (2006) are based on Argo data which are relatively
75 sparse in space and time. In particular, KS20 cannot co-locate the BLs relative to the concurrent
76 position of the North Equatorial Counter Current (NECC) or any property front associated with
77 the circulation system, nor do they shed any light on what specific dynamics may be occurring at
78 the front associated with BL formation. Indeed, it is difficult to obtain the direct measurements
79 of the 3-dimensional circulation and air-sea interaction that are needed to determine the
80 mechanisms responsible for BL formation using an *in situ* dataset.

81 Katsura et al. (2020) looked in more detail at BL and temperature inversion formation
82 using the higher resolution SPURS-2 (Salinity Processes in the Upper ocean Regional Studies –
83 2) *in situ* dataset. They reached a similar conclusion as KS20, that BLs form as a result of tilting
84 of mixed layer fronts. Additionally, they surmise that BLs form in a patchy and intermittent
85 manner on fast time scales and that surface geostrophic flow and Ekman flow play important
86 roles in causing the tilting of frontal isohalines - where BL formation occurs. However, Katsura
87 et al. (2020) is based on shipboard observations, so temporal changes in BLs cannot be described
88 even though synoptic BL features were observed.

89 The ETP is the location of the seasonal extension of the ETP fresh pool (Alory et al.,
90 2012; Melnichenko et al., 2019), a low surface salinity feature which extends westward from the
91 coast of Central America. It reaches its maximum extent in the October/November period,
92 reaching out to $\sim 160^\circ\text{W}$, as defined by the 34 isohaline, with minimum extent in
93 January/February at $\sim 125^\circ\text{W}$. Its meridional extent, again defined by the 34 isohaline, is about
94 10° in the mean between about 5 and 15°N (Guimbard et al., 2017; Fiedler and Talley, 2006). At
95 the southern edge of this fresh pool extension is a surface front separating the relatively fresh
96 eastern Pacific water from higher salinity surface water found at the equator. This front forms in
97 January near $\sim 3^\circ\text{N}$, migrates to the north over the course of the year, and dissipates in the months
98 of January-February after reaching a maximum latitude of about 12°N (Yu, 2015). In the
99 October-November period it is generally found around 6 - 7°N , which is one location where the
100 present study will focus. The ETP is unique due to the intense currents, strong fronts, dominance
101 of Ekman transport, and shallow mixed layers that are present. These all likely point to the
102 CM02 tilting mechanism as the most important one for BL formation. BLs in the ETP are
103 generally thinner than in the western Pacific (Fiedler and Talley, 2006). The ETP is also a site of
104 intense rainfall (Schanze et al., 2010). However, according to KS20, rainfall and BLs do not

105 generally coincide, meaning that rainfall may not be an important mechanism contributing to the
106 formation. Thus, we would like to look at the tilting mechanism in the ETP in more detail.

107 Using a numerical model, we can focus in on the mechanisms responsible for BL
108 formation, and examine how or whether the BL formation is related to 3-dimensional frontal
109 structures and their temporal evolution. As stated by Tanguy et al. (2010), a complete
110 understanding of BL formation requires information “on the 3-dimensional structure of the upper
111 ocean, T, S, velocity, vertical shear, local surface forcing and turbulent mixing”. BL formation in
112 numerical models has been studied by Veneziani et al. (2014) in the South Atlantic, using the
113 same model formulation we use here, though configured specifically for that different region.
114 They emphasized the importance of advection, and, importantly, of the influence from
115 submesoscale processes at 1-9 km spatial scales and their impact on vertical transport of heat and
116 salt. The ETP was the location, in 2016-2017, of the SPURS-2 field campaign (Lindstrom et al.
117 (2019) and references therein), carried out to study the impact of rainfall on the upper ocean
118 salinity field, and the creation of the Pacific basin-wide low sea surface salinity (SSS) feature
119 (e.g. Schanze et al., 2010). Associated with the field campaign, there was an effort to simulate
120 the dynamics in a regional ocean model based on the Regional Ocean Modeling System (ROMS;
121 Li et al., 2019, henceforth “Li19”; Shchepetkin and McWilliams 2011).

122 In this paper, we study BL formation in a couple of individual events within the high-
123 resolution ROMS daily output. The ROMS output displays BLs in the ETP, which can be related
124 to surface circulation, surface convergence, salinity, winds and freshwater forcing from the
125 atmosphere. ROMS allows us to examine the processes involved in BL formation at a scale and
126 level of detail that is not possible with in situ data. Also, while BLs have been frequently studied
127 in the western Pacific, less is known about their characteristics and formation mechanisms in the
128 ETP where forcing is much more seasonal as it is aligned with the seasonal march of the ITCZ.
129 The choice of events to study was somewhat arbitrary. We wanted to look at one instance that
130 could be directly compared to data collected during the SPURS-2 field campaign and another
131 event that was relatively isolated and long-lived. These events are not necessarily typical.
132 However, by studying a couple of individual instances, we may be able to infer more broadly
133 about how BLs relate to the dynamics of the ETP fresh pool and its seasonal extension across the
134 Pacific.

135

136 **2 Data and Methods**

137 **2.1 ROMS Simulation**

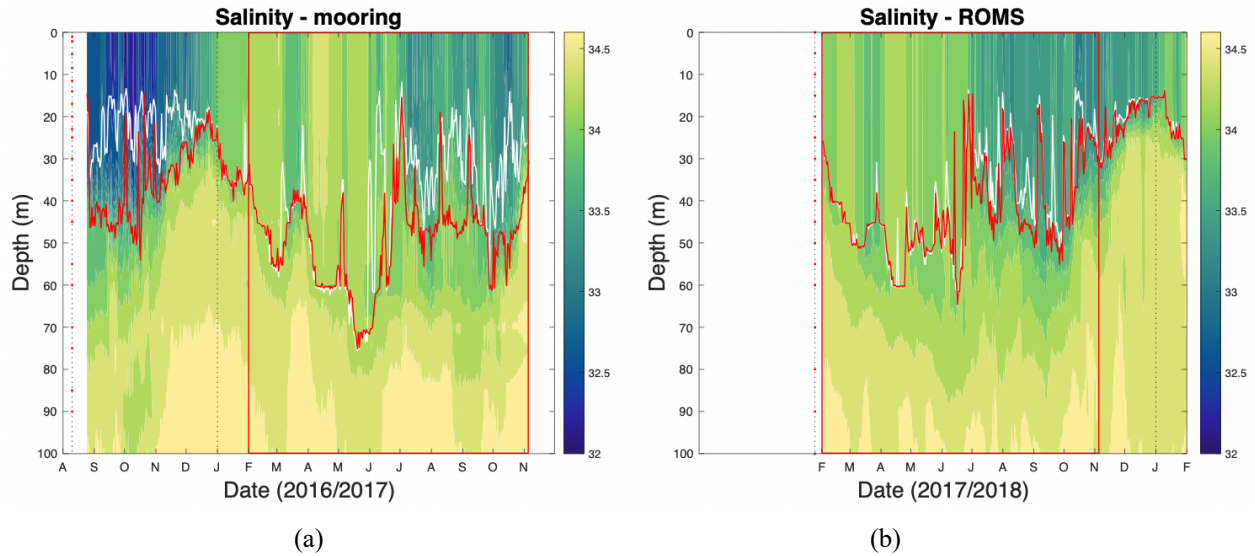
138 The ROMS simulation (Li, 2020) uses data assimilation to constrain the large-scale and
139 large mesoscale circulations as a method for more realistically reproducing BL formation. The
140 model is nested in three levels, 9 km, 3 km and 1 km (see Figure 2 in Li19). We use the 3 km,
141 middle level, with daily average output. In the vertical, the model has 52 levels. To effectively
142 resolve dynamical processes associated with BL formation 22 of those are within the top 100 m,
143 with the topmost level at 1 m. Model output was interpolated onto a set of standard levels to do
144 the calculations discussed and displayed in this paper (Figure 1b). The model covers the time
145 period 1 February 2017 – 31 January 2018, whereas the SPURS-2 field campaign went from late
146 August 2016 to early November 2017. Thus, the model and field campaign overlap for about 9
147 months of 2017 (Figure 1).

148 The atmospheric forcing for ROMS is derived from the 18 km resolution NCEP GFS
149 (National Centers for Environmental Prediction Global Forecast System) operational
150 atmospheric model output. A bulk flux formula (Fairall et al., 2003) is used to calculate the
151 forcing. The inputs include 3-hourly atmospheric fields of 10-m wind speed and direction, net
152 shortwave radiation, downward longwave radiation, 2 m air temperature, 2 m relative humidity,
153 and precipitation. Rainfall in this region tends to come in very heavy and patchy downpours
154 whose sizes are on the order of a few km (Rutledge et al., 2019; Thompson et al., 2019). The 18
155 km resolution of the model forcing does not allow one to distinguish these individual rain events
156 and thus changes to SSS associated with convective rainfall are not represented in the ROMS
157 simulation.

158 The model assimilates a number of datasets. One of these is the monthly-average data
159 from version 4 of the Met Office Hadley Centre “EN” series (Good et al., 2013). This monthly
160 dataset constrains three-dimensional T/S fields on spatial scales larger than 400 km and thus is
161 used to reduce model bias. Another assimilated dataset is the gridded AVISO (Archiving,
162 Validation and Interpretation of Satellite Oceanographic data) sea surface height product. This
163 product has a grid of 0.25° , but the effective resolution is about 300 km (Pujol et al., 2016).
164 Satellite SST measurements from the Advanced Microwave Scanning Radiometer-2 (AMSR-2),
165 a passive microwave radiometer flying on NASA's Aqua satellite, are also assimilated. The
166 AMSR-2 SST has a resolution of 0.25° . Using the multi-scale scheme as described in Li et al
167 (2015, 2019), the data assimilation is configured to primarily constrain eddies and circulation
168 with spatial scales larger than 300 km. There are no SPURS-2 in situ observations assimilated in
169 this 3 km model domain.

170 Real-time forecasts of the modeling system during the SPURS-2 field campaign have
171 been encouraging. As presented in Li19, a range of evaluations showed the modeling system
172 predicted the time evolution of the mesoscale circulation compared to measurements of SSH,
173 SST and surface currents. For example, the 2-day SSH forecast had a spatial correlation larger
174 than 0.9 and a root-mean-square error (RMSE) of less than 4 cm against the AVISO gridded data
175 product on a daily basis, and the model SST forecast had a RMSE of 0.6°C against observations
176 from as many as 130 drifters. The vertical T/S profiles are comparable to the observed. As such,
177 we are convinced that the BLs that the model produces essentially represent the same dynamical
178 processes that are responsible for the generation of the observed BLs.

179 From the model output, we computed such quantities as divergence and vorticity.
180 Isothermal layer depth (ILD) and mixed-layer depth (MLD) were determined using the method
181 of deBoyer Montegut et al. (2007). In that paper, the ILD (their “ D_{T-02} ”) is defined as the depth
182 where potential temperature is greater than that at a reference depth by 0.2°C . The MLD (their
183 “ D_σ ”) is the depth where “the potential density ... has increased from that at the reference depth
184 by a threshold ... equivalent to the density difference for the same temperature change at
185 constant salinity”. They use a reference depth of 10 m, but here we use 0 m. BL thickness (BLT)
186 is the difference between ILD and MLD when that difference is greater than zero.



187

188

189 Figure 1. Time series of salinity vs. depth observed at (a) the SPURS-2 central mooring
 190 ($10^{\circ}\text{N}, 125^{\circ}\text{W}$) (Farrar, 2020) and from (b) the corresponding grid cell in the ROMS simulation.
 191 ILD is in white and MLD in red. The difference between them is the BLT. Color scales are at
 192 right for each panel. Also note these two panels do not cover the same periods. Mooring salinity
 193 covers the period August 2016 – November 2017, whereas the ROMS salinity is computed over
 194 February 2017 – January 2018. A red box in each panel outlines the overlapping time period,
 195 February–November 2017. At the left of each panel are vertically-arranged red dots showing the
 196 locations of the mooring instruments above 100 m in panel (a) and the ROMS interpolated
 197 vertical levels above 100 m in panel (b).

198

2.2 In situ data

199 Brief use is made in this paper of data (Farrar, 2020) from the SPURS-2 central mooring
 200 (Figure 1a). See Farrar and Pluedemann (2019) for a description of the methods associated with
 201 this dataset.

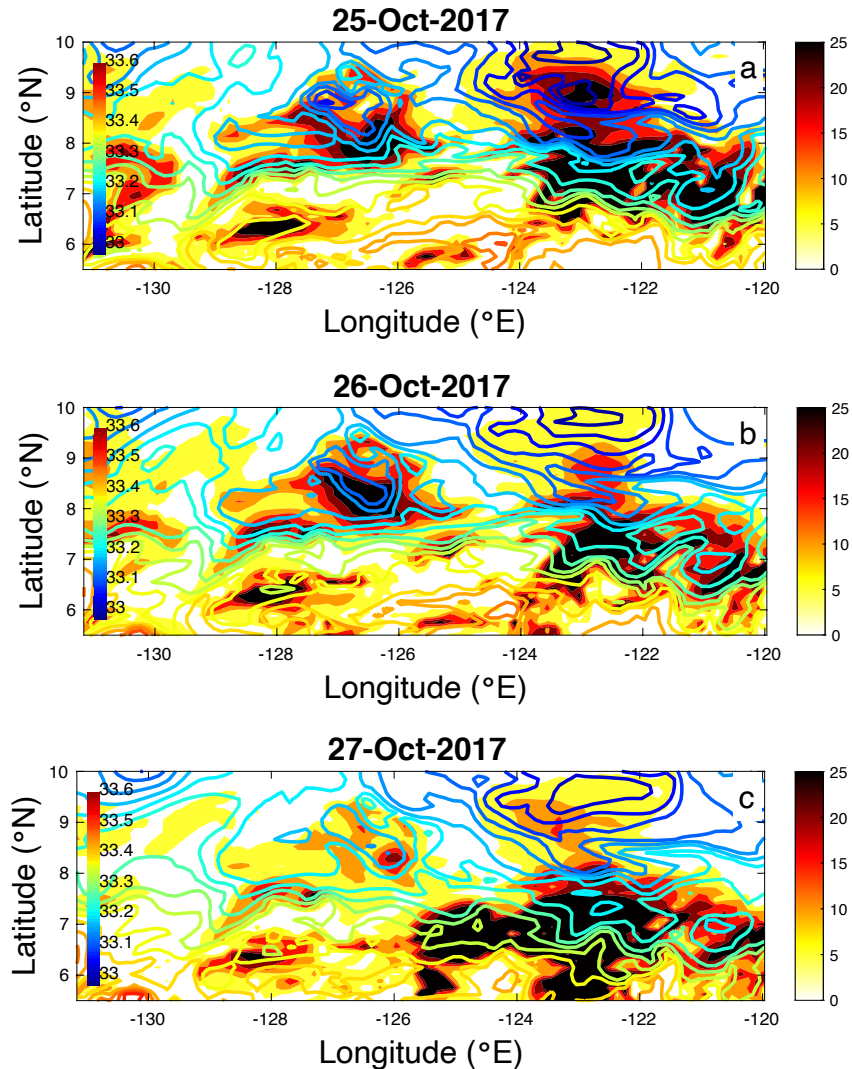
202 Brief use is also made below of underway CTD (uCTD) data from SPURS-2 (Sprintall,
 203 2019a,b). These data have vertical resolution of about 6 m. For the section we display below, the
 204 horizontal resolution is about 0.1° along-track (Katsura et al., 2020).

205 3 Results

206 In the supporting information we include an animation of BLT within the model during
 207 the SPURS-2 period along with SSS (Animation S1). Thick BLs are often generated within
 208 eddies (e.g. 8-Feb – 20-Feb-2017 at $12.5^{\circ}\text{N}, 124^{\circ}\text{W}$) or across strong fronts (e.g. 12-May – 22-
 209 May-2017 at $13^{\circ}\text{N}, 125^{\circ}\text{W}$). These BLs can persist for days or weeks, or appear and disappear in
 210 a day or two (e.g. 31-July – 1-August-2017). They can be isolated in time and space, or be
 211 ubiquitous throughout a large part of the domain shown (e.g. 29 June 2017). BLs appear in the
 212 model output, but they are not generally as thick or persistent as those in the *in situ* data. This is
 213 evident through a comparison (Figure 1) between model output and observed T/S data from the
 214 SPURS-2 central mooring. Note the ubiquitous presence of 20-30 m thick BLs in late summer
 215 and fall in the mooring data which are either absent or more sporadic in the ROMS simulation.

216 3.1 October Event

217 Thick BLs are present intermittently along an SSS front south of 10°N that persists for
 218 much of October and November (Animation S1). Figure 2 shows this for a three-day period near
 219 the end of October. A strong relationship is seen between SSS fronts and BLs. Thick BLs are
 220 often present on the fresh side of a front. Examples are seen at 7.5°N,128°W, or 7°N,123°W on
 221 all three days. Some of these features are persistent over the three-day period (e.g.
 222 7.5°N,128°W). Others evolve rapidly, either dissipating (e.g. 8.5°N,127°W), or suddenly
 223 appearing (e.g. 6.5°N,125°W). It's this last feature that we will now study in detail as it
 224 develops.

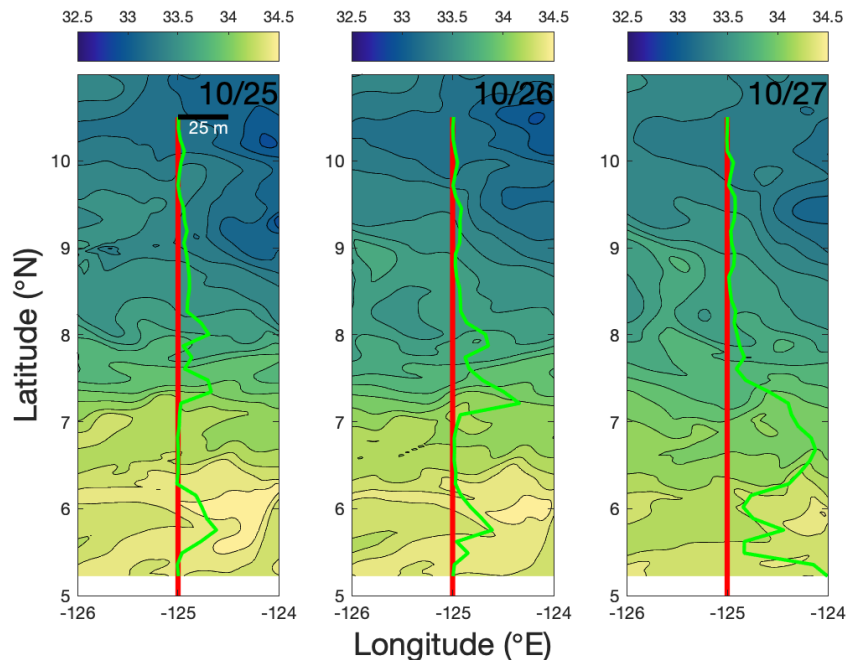


225 Figure 2. Contours: SSS with color scale at left. Shading: BLT in meters with color scale at right.
 226 a) 25-October. b) 26-October. c) 27-October.

227 On 27-October-2017 there is a very thick BL around 6-7°N from 126°W to 120°W
 228 (Figure 2c). It does not seem to be connected to BLs seen further west in the prior days, as the
 229 current speeds are not fast enough for advection to work. Much of the model domain south of
 230 8°N on 27-October shows BLs that are >25 m thick. These thick BLs are associated with a

231 complex SSS front that snakes through the region from (6°N,120°W) to (7°N,129°W)
 232 (Animation S1, Figure 2c) on this day. On 27-October the BL is centered at about 6.75°N, but is
 233 relatively thick from 6°N to 7.5°N along 125°W (Figure 3 right panel). What is clear from the
 234 SSS is the low salinity water spreading to the south during the prior two days. The SSS front
 235 relaxes and becomes more diffuse at 125°W as seen in the contrast between 26 and 27 October
 236 as seen in Figures 2 and 3 and Animation S1. Water in the vicinity of the thick BL is much
 237 fresher on 27-October than the two previous days (Figure 3a, b) when no or minimal BLs
 238 existed.

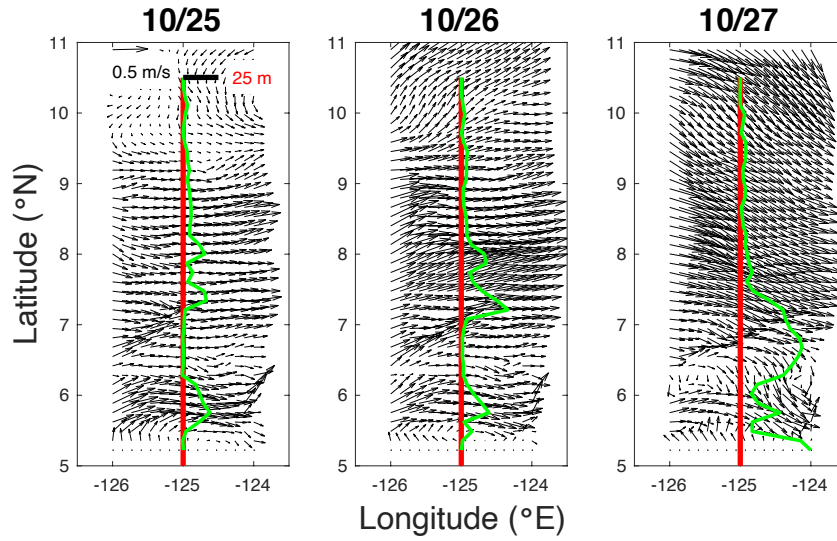
239



240
 241

242 Figure 3. SSS from the ROMS domain on (left panel) 25, (center panel) 26 and (right panel) 27
 243 October 2017. Color scale is at the top. Red line is along 125°W. The thick green line represents
 244 the BLT at 125°W at a given latitude, where zero BLT is the red line and 25 m BLT is indicated
 245 by the scale bar at 10.5°N in the left panel.

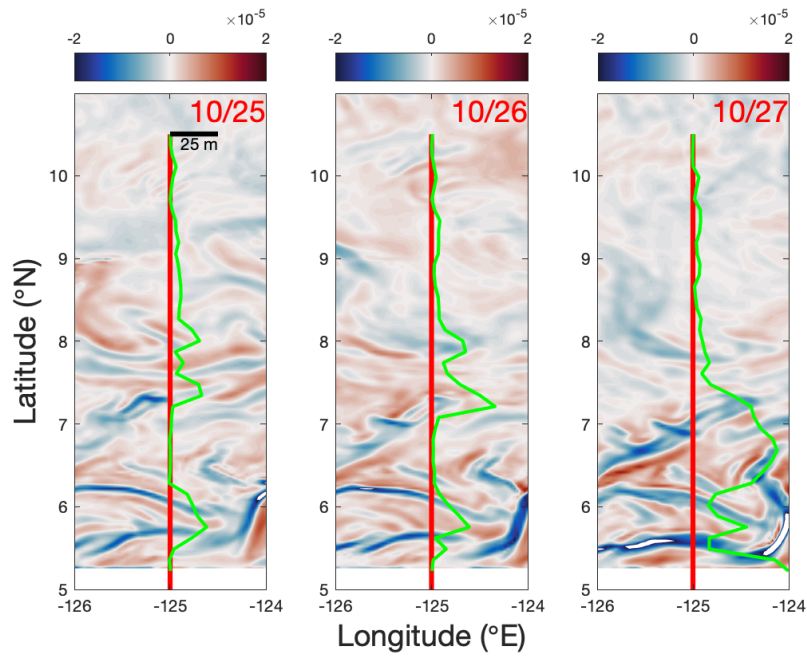
246 The ocean current vectors (Figure 4) on 27-October show water flowing eastward
 247 throughout the entire domain. The thick BL of 27-Oct is associated with the sharply decreased
 248 SSS brought about by advection and the southward motion of a SSS front. A convergent feature
 249 is evident in the northern part of the region of thick BLs around 7°N (Figure 4 right panel). Just
 250 to the south of this convergent feature is an area of divergence near the center of the area of thick
 251 BL. This same convergent feature has migrated over the previous two days when it is also
 252 associated with thick BLs, although not as thick as on 27 October (e.g. 7.2°N on 26 October). So
 253 thick BL formation in this instance appears to be associated with surface convergence and
 254 divergence.



255

256 Figure 4. As in Figure 3, but for current velocity vectors. A scale arrow is at the top left in the
257 left panel.

258



259

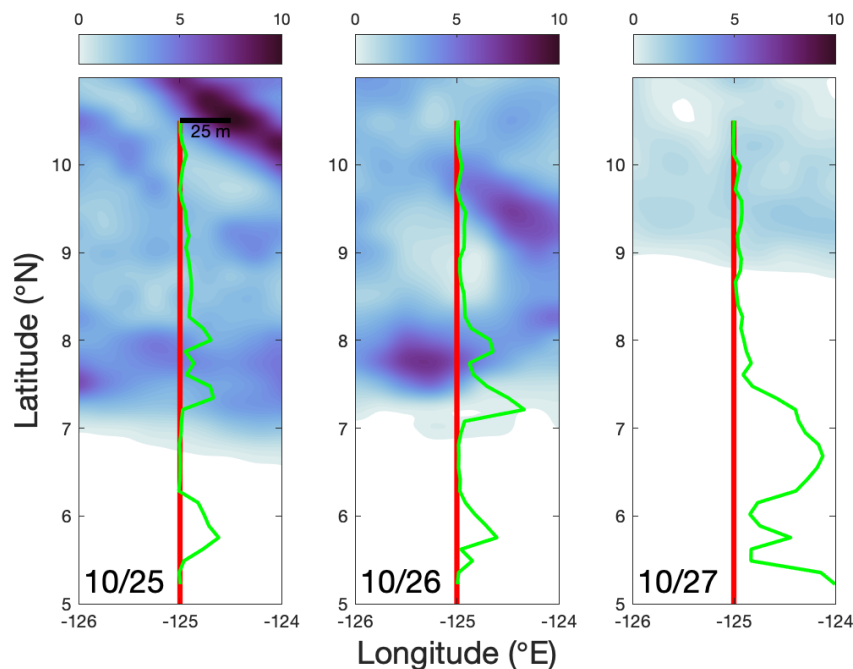
260 Figure 5. As in Figure 3, but for horizontal divergence. Color scale is at the top of each panel in
 261 units of s^{-1} .

262

263 The thick BLs on all three days are associated with areas of intense surface divergence
 264 and convergence culminating on 27 October (Figure 5 right panel). The thickest BLs are
 265 associated with surface divergence on the fresh side of the front and there is some indication that
 266 surface convergence is associated with reduced BLT (e.g., $5.5^{\circ}N$ and $6^{\circ}N$ on 27 October). There
 267 are also places where thick BLs are associated with alternating surface convergence and
 268 divergence, for example around $6^{\circ}N$ on 25 October and $7.25^{\circ}N$ on 26 October. It should be
 269 noted here that we have examined other variables such as SST and vorticity over large scales.
 270 Divergence seems to have the most consistent relationship with BLs such as is seen in Figure 5.

271 The precipitation forcing the model is very small on 27 October and far removed from
 272 where the thick BLs are formed (Figure 6, right panel). An area of heavy precipitation is located
 273 at ($7.75^{\circ}N, 125.5^{\circ}W$) on 26 October which may have had an influence on the thick BLs at $6.75^{\circ}N$
 274 the following day, though this is not obvious from the SSS shown in Figure 3. Note that this map
 275 of precipitation is very smooth compared to the ones of Thompson et al. (2019) and Rutledge et
 276 al. (2019) from the same region and time period, and has larger scales of variability.

277



278

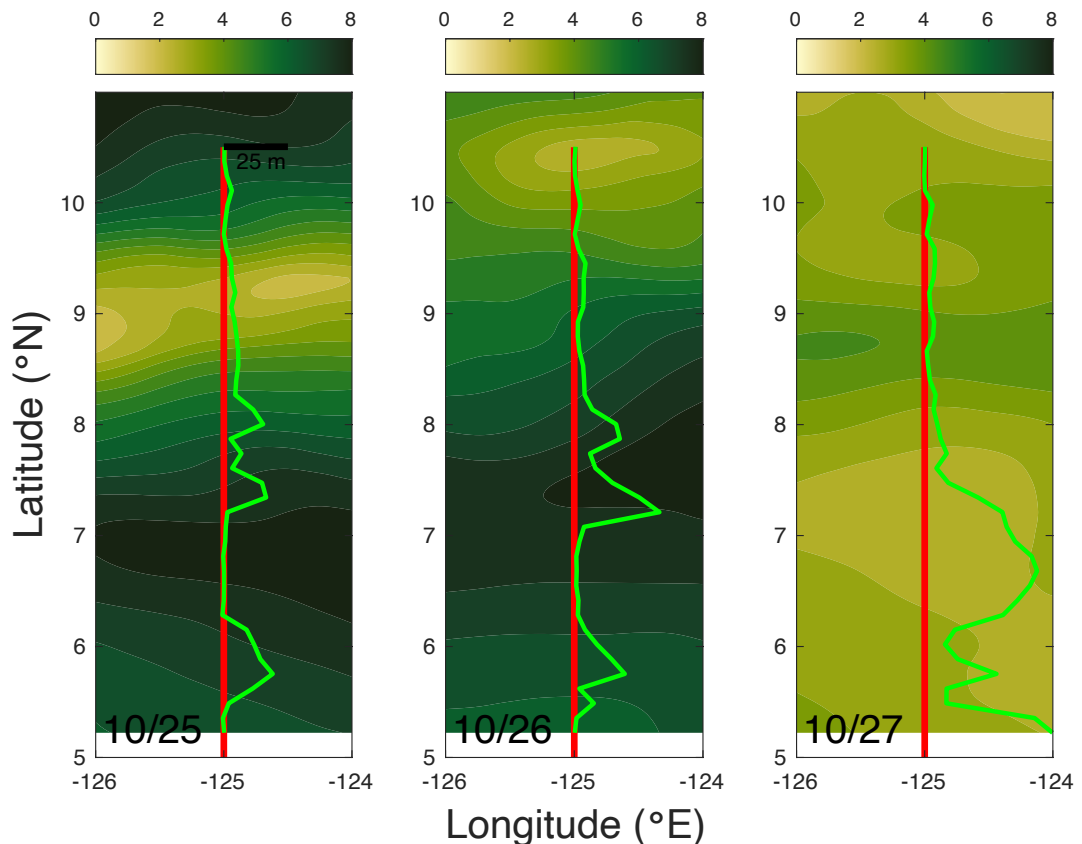
279 Figure 6. As in Figure 3, but for daily average precipitation rate. Color scale is at the top for each
 280 panel in units of $mm\ hr^{-1}$.

281 Wind speed undergoes a rapid change from 25-26 October to 27 October (Figure 7). On
 282 27 October, the winds were nearly calm, whereas in the region of thick BL the winds were up to

283 8 m s⁻¹ on the previous two days. The winds on 25-26 October were mainly out of the south (not
 284 shown). Perhaps the sudden change in the winds allowed low SSS water at the surface to drift
 285 southward after the change.

286

287



288

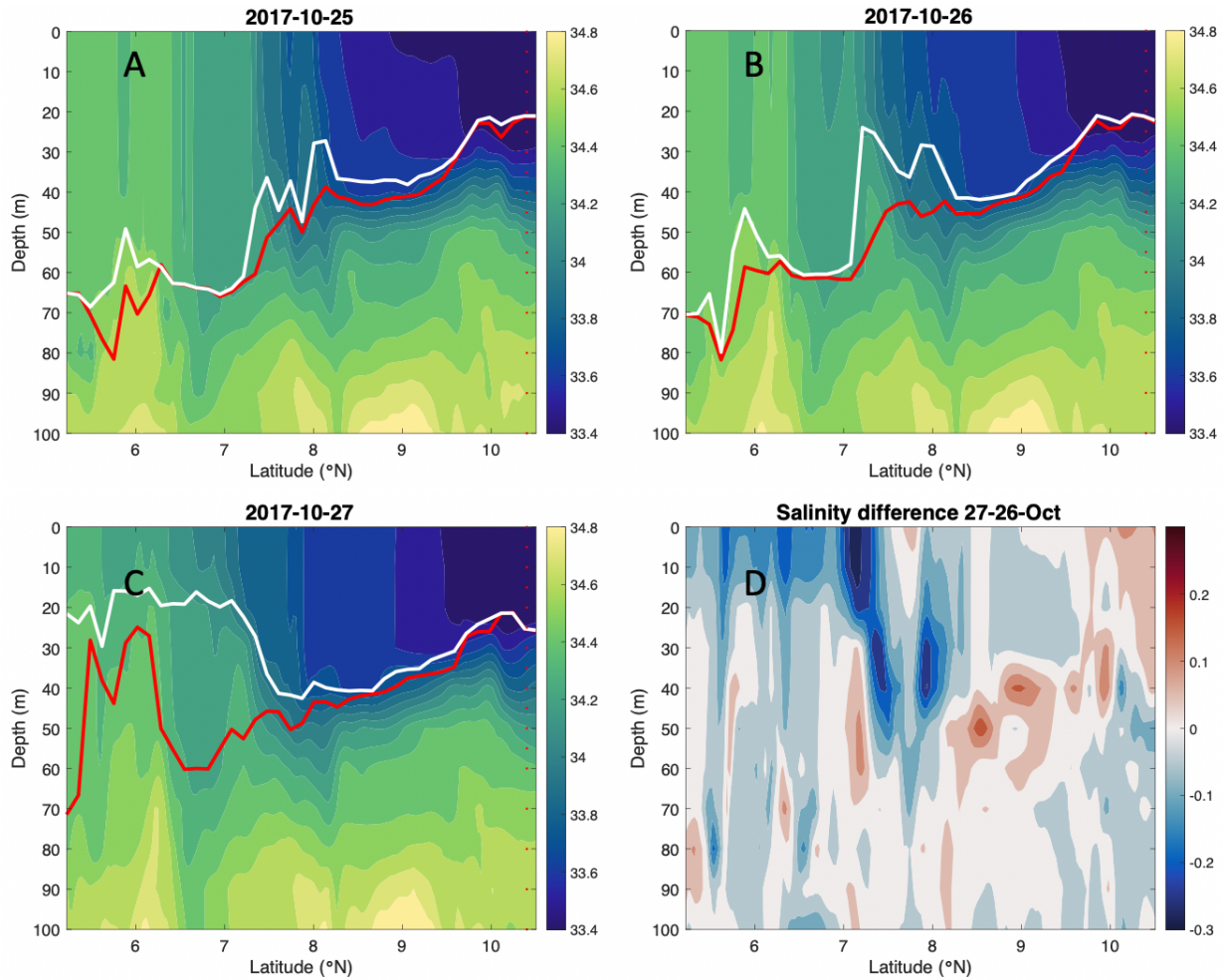
289 Figure 7. As in Figure 3, but for surface wind speed. Color scale is at the top for each panel in
 290 units of m s⁻¹.

291

292 A meridional section along 125°W (Figure 8) shows fresh surface water spreading across
 293 the area between 6 and 7°N and the generation of a thick BL. On 25 and 26 October, there is a
 294 thin BL between 7 and 8°N (Figure 8a and b). By 27-October, relatively fresh surface water had
 295 spread southward to around 6°N (Figure 8c). This spreading occurred in the upper 20 m as
 296 evident in the large salinity difference shown in Figure 8d. The spreading left a thick BL
 297 between 6.25 and 7.5°N. South of there, between 26 and 27 October, the ILD shoaled from 60 to
 298 30 m. What we see here is somewhat like the tilting of isohalines posited by CM02, but it is not
 299 exactly the same. In the main, the isohalines tilt during the days shown, but the tilting goes on
 300 mostly below 20 m depth. That is, the base of the isohalines tilts, but the upper part remains
 301 vertical. The salinity front at 7.5°N relaxes and spreads southward. CM02 implied that BLs are

302 generated by current shear which causes the tilting (see their Figure 1). A complicating fact is
 303 that the zonal flow is much stronger than meridional. Perhaps in this case the tilting is not caused
 304 by cross-front vertical shear, but by some other mechanism.

305



306

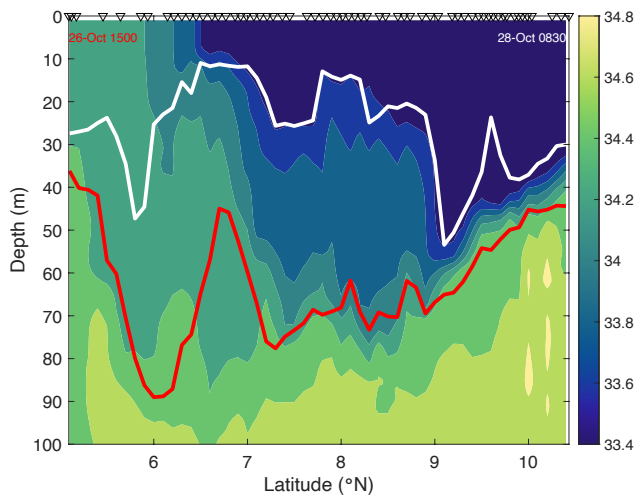
307

308 Figure 8. ROMS Salinity sections along 125°W for (a) 25 October, (b) 26 October and (c) 27
 309 October. Each panel represents a daily average centered at 1500 Z each day. Color scales are at
 310 right. Small red dots near the right side of panels a-c are the locations of the model levels used in
 311 this paper. Thick red line is the ILD, while thick white line is the MLD. (d) Difference between
 312 panels (c) and (b).

313

314 October 2017 coincided with one of the two main SPURS-2 cruises. A uCTD section to
 315 ~250 m was obtained along 125°W from 10.5 to 5°N on 26-28 October (Figure 9). This uCTD
 316 section also showed that a thick BL existed, but it was much thicker (~50 m) and more extensive
 317 (from 9° to 6°N) than that produced in the ROMS output (Figure 8). There is a salinity front at
 318 the surface near 6.5°N. We also see the same configuration of the front, vertical isohalines at the
 319 surface and tilted ones below it as was observed for the model. The difference here is that the BL

320 is much thicker in the uCTD data and the part of the water column with vertical isohalines much
 321 thinner. Katsura et al. (2020) show a similar section from a few days later, 3-5 November.

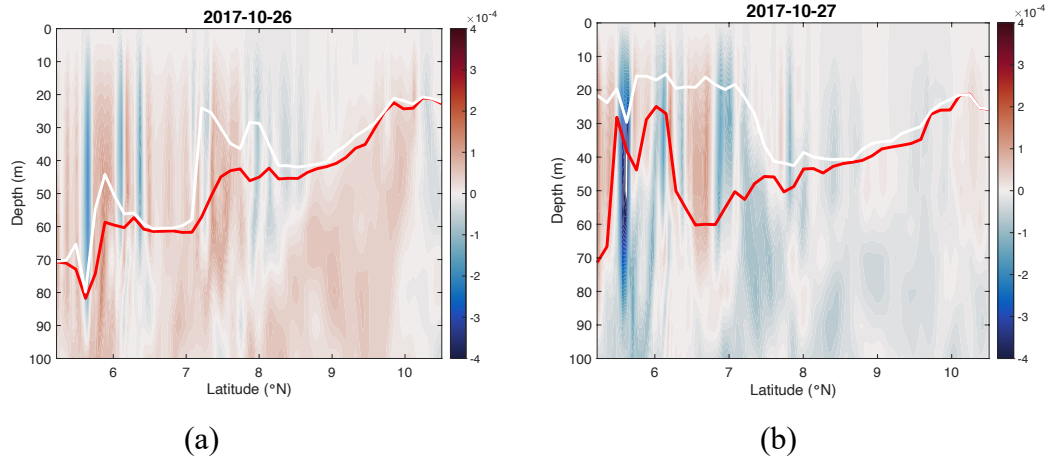


322

323 Figure 9. Salinity section from uCTD data (Sprintall, 2019a,b) along 125°W collected on the
 324 R/V Roger Revelle, 26-28 October 2017. Color scale is shown at right. Thick red line is the ILD,
 325 while thick white line is the MLD. Vertical resolution of uCTD data is ~6 m. Dates and times
 326 shown at the top left and right are for the first and last casts. Thus, the section data were
 327 collected as the ship moved from south to north and took about 1.7 days to complete. Inverted
 328 triangles at the top are the locations of the casts – there were 62 of them.

329 It is clear from Figures 4 and 5 that the presence of BLs is strongly related to surface
 330 horizontal divergence/convergence. Thus, because divergence and convergence are usually
 331 accompanied by vertical motion, it is likely related to vertical processes such as vertical flows,
 332 mixing and entrainment. The vertical velocity along 125°W (Figure 10) shows alternating bands
 333 of strong upward and downward flow in the mixed layer south of 7.5°N on 27 October. As
 334 expected, these bands are directly related to the maps of surface divergence (Figure 4), upward
 335 flow occurs where there is surface divergence and downward flow where there is convergence.
 336 The strong flow ceases at the base of the mixed layer, except for one band of downward flow at
 337 5.6°N. For the most part, where the BL is thickest, the flow is upward. Where vertical velocity is
 338 minimal, north of 8°N, BLs are thin to non-existent. This pattern is repeated at 5.5-6°N and 7.5-
 339 8°N on the previous day (Figure 10a).

340



341

342

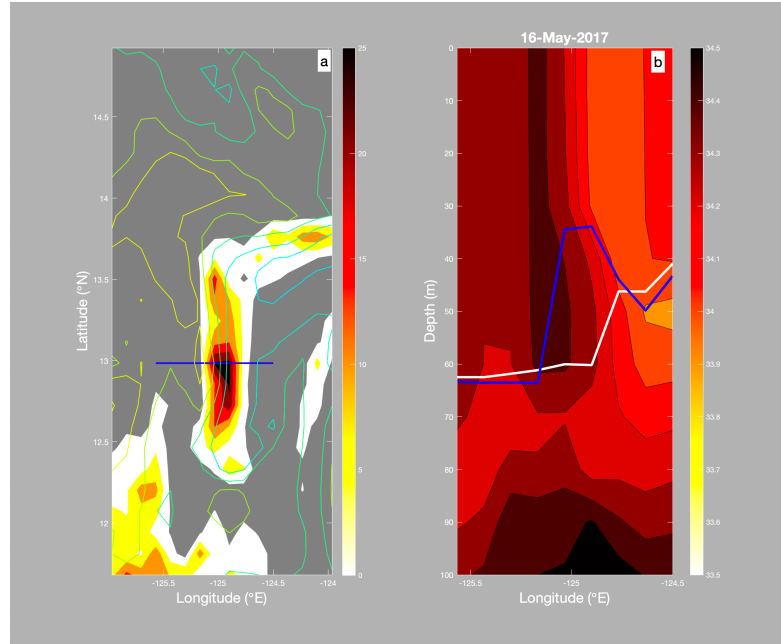
343 Figure 10. Vertical velocity sections along 125°W for (a) 26 and (b) 27 October. Color scales (in
 344 m/s) are at right. Red colors are upward and blue downward. Thick red line is the ILD, while
 345 thick white line is the MLD.

346

347 3.2 May Event

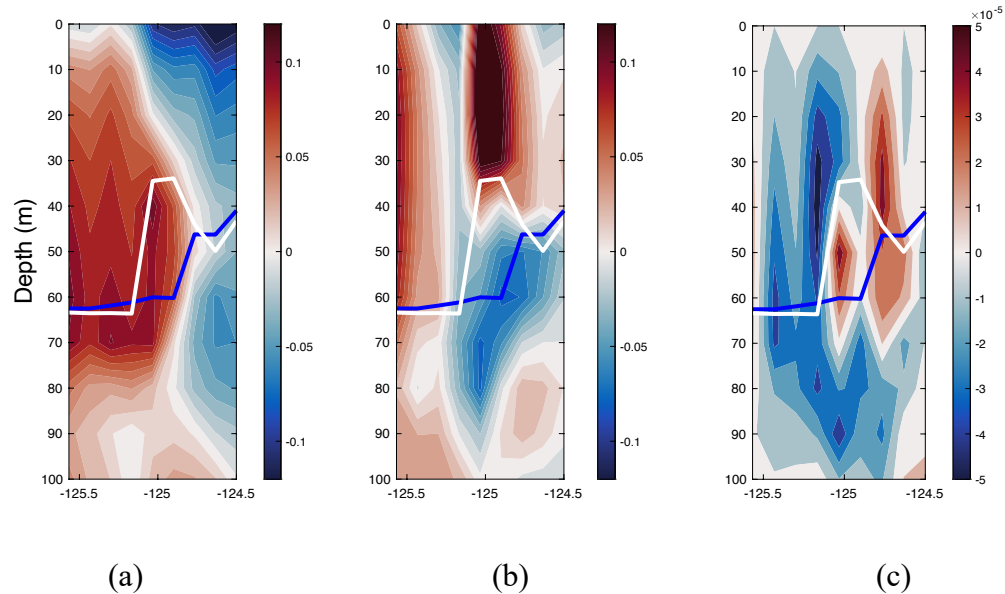
348 Between 7 and 26 May 2017, especially starting around 9 May, a BL developed across a
 349 north-south oriented front between 12 and 13°N near 125°W (Animation S1). This BL reached a
 350 maximum BLT of more than 25 m and persisted for more than two weeks within the front,
 351 eventually migrating northward to turn to an east-west orientation further north before
 352 dissipating by 30-May. The BL is clearly evident in the horizontal plan view (Figure 11a,
 353 Animation S2). Similar to the October event, there is tilting of isohalines (Figure 11b). The BL is
 354 situated on the low salinity side of the front at 125°W, with fresher water to the east. The front is
 355 tilted in the vertical, but not uniformly. All of the tilting occurs at the base of the front between
 356 30 and 60 m depth, similar to that found in the October event (Figure 8c). The horizontal
 357 velocity field shows a tilting convergent strip that is close to the front near the surface, but tilts
 358 through the front to the fresh side with depth (Figure 12a), with the strongest convergence being
 359 at the front base at a depth of 60-70 m. The vertical velocity (Figure 11c) has upwelling (red
 360 color) just below the surface decreasing to zero at the surface on the fresh side of the front
 361 indicating surface divergence. On the opposite side of the front there is downwelling below the
 362 surface (blue color) decreasing to zero at the surface indicating surface convergence (Figure 13).
 363 At the base of the ML, the sense of change of vertical motion changes, implying convergence at
 364 the base of the ML on the fresh side of the front and divergence on the salty side. It should also
 365 be noted that no rainfall fell anywhere near the location of this front in this time period, and that
 366 examination of the distribution indicated no strong front in temperature as there is in salinity.
 367 The temperature difference between the salty and fresh side of the front is at most ~0.1-0.2°C,
 368 with the salty side being colder.

369



370

371 Figure 11. BLT and salinity on 16 May 2017 extracted from Animation S2. a) Plan view.
 372 Colored contours: SSS with contour interval 0.1. High SSS in yellow and low SSS in blue.
 373 Colors: BLT with color scale at right. Grey color indicates zero BLT. Blue line is the location of
 374 the vertical section displayed in the right panel. b) Vertical salinity section across the front in the
 375 left panel. Blue line is the ILD. White line is the MLD. The difference between them is the BLT.

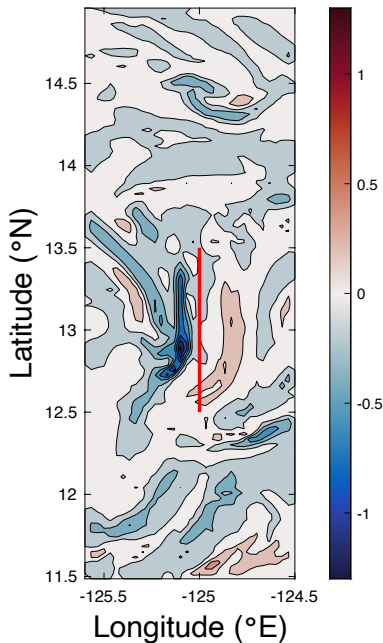


376

377

378 Figure 12. a) Zonal velocity (m/s) along the same section as in Figure 11 right panel for 16 May
 379 2017. White line is the MLD and blue line is the ILD. Red (blue) colors indicate positive
 380 (negative) velocity, or to the left (right) in the section. b) Same as panel a), but for meridional

381 velocity. Red (blue) colors indicate flow northward or into the page (southward or out of the
 382 page) c) Same as panel a) but for vertical velocity. Upward flow in red colors, downward in blue.



383

384 Figure 13. Surface divergence on 16 May 2017. Units are 10^{-5} s^{-1} with color scale at right. A
 385 vertical red line indicates the approximate position of the sharpest part of the SSS front in Figure
 386 11.

387

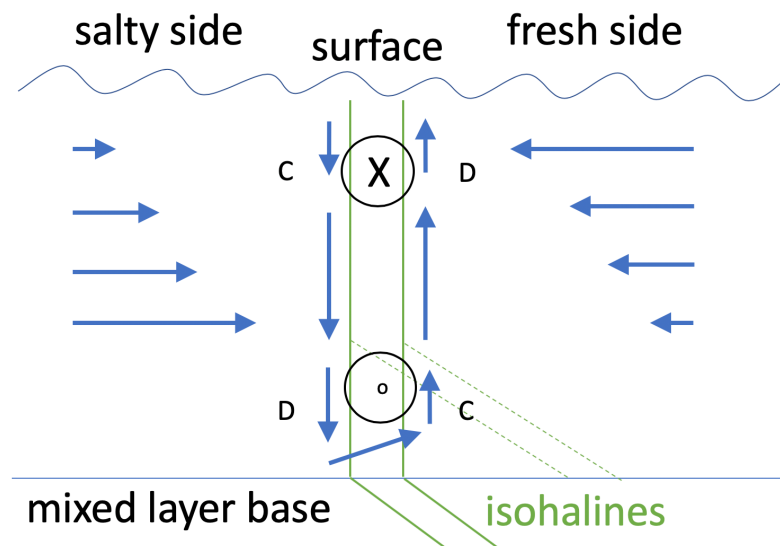
388 4 Summary and Discussion

389 Using a version of ROMS set up for the SPURS-2 region in the eastern tropical Pacific
 390 Ocean, we have studied two events when BLs appeared in the model. Both events were
 391 associated with sharp mixed layer salinity fronts. The first occurred at 6-7°N in October 2017,
 392 and was part of a complex of BLs formed along a large-scale front. The other occurred at 12-
 393 13°N in May 2017, at the leading edge of the extension of the EPFP. In each case, a thick BL
 394 was created when the bottom part of a salinity front tilted towards the fresh side of the front. In
 395 the October event, the formation of the BL was associated with spreading of fresh over salty
 396 water and motion of the salinity front. In the May event, the front remained relatively stationary,
 397 and persisted for more than two weeks.

398 The hypothesis of KS20 and CM02 is that BLs can be formed by tilting of vertically-
 399 oriented isohalines by shear flow at a mixed layer salinity front. The analysis of the May and
 400 October events suggests a modified version of this mechanism (Figure 14) that the full
 401 concurrent property and velocity fields from the model simulation enable us to better resolve
 402 compared to *in situ* observations. This starts with a vertical front of salinity in the mixed layer.
 403 On the fresh side of the front the flow is horizontally divergent at the surface, and pulls water up
 404 from the mixed-layer base. On the salty side of the front, the flow is convergent at the surface,
 405 and pushes water down into the mixed layer. The opposite is the case at the base of the mixed

406 layer, with divergence on the salty side and convergence on the fresh side. Thus, a small vertical
 407 circulation cell is set up with water flowing across the front at the mixed layer base from the
 408 salty to the fresh side. At the base of the mixed layer, the isohalines then tilt generating the BL
 409 that is observed. The mixed layer front is accompanied by a strong vertical shear through the
 410 thermal wind relation. This vertical shear may play a role in generating and maintaining the
 411 horizontal convergences and divergences that drive the vertical circulation (KS20). In particular,
 412 the surface divergence on the fresh side of the front may be due to acceleration of the flow by
 413 concentration of the front's isohalines at the location of the BL (Figure 12b).

414 CM02 postulated that a strong salinity gradient can generate a shear flow across the front
 415 and tilt the isohalines in the absence of other processes that might balance the pressure gradient.
 416 Perhaps there are other processes occurring at the surface (e.g. turbulent mixing or wind stress)
 417 that can balance the pressure gradient keeping the front vertical there, but not at the base of the
 418 ML. Maybe the front itself generates along-front vertical shear (Figure 12b) as it forms through
 419 the thermal wind relation which is able to balance the across-front pressure gradient near the
 420 surface but not as much at the ML base. The front shown in Figure 11 is there for a long enough
 421 time to become geostrophically balanced, and so the thermal wind relation holds there, and the
 422 across-front shear is much stronger near the surface than at the ML base (Figure 12a).



423

424 Figure 14. Schematic view of proposed BL formation mechanism in the ETP showing a section
 425 across a zonal salinity front in the mixed layer as in Figure 11b. The zonal velocity, the arrows at
 426 the left and right, indicate a tilting shear flow. On the salty side of the front there is horizontally
 427 convergent flow at the surface and divergent flow at the base of the mixed layer. By contrast, on
 428 the fresh side there is divergent flow at the surface and convergent flow at the base of the mixed
 429 layer. This sets up a vertical circulation that acts to tilt isohalines mainly at the front's base
 430 (dashed lines) and generate a thick BL. Included is a strong vertical shear parallel to the front
 431 (into/out of the page) which helps to maintain the vertical orientation of the front at the surface
 432 and contribute to the convergent and divergent parts of the flow.

433 The proposed mechanism shown in Figure 14 is two-dimensional. However, it greatly
 434 simplifies the mesoscale surface circulation that in reality generates and moves the front and
 435 associated convergence/divergence, and it ignores mixing and entrainment of salt through the

436 base of the mixed layer. The schematic does however, place emphasis on vertical processes in
437 the vicinity of a front, which seems appropriate given the apparent association between BL
438 formation, horizontal divergence and the presence of fronts (KS20). Indeed, Vialard and
439 Delecluse (1998b) suggest a similar mechanism, including downwelling near the front, but
440 emphasize the role of precipitation to a greater degree. That study was conducted in the western
441 tropical Pacific where precipitation may be more important in the BL formation process.

442 KS20 emphasize the importance of Ekman transport in the formation of BLs, especially
443 in summer and fall in the eastern tropical North Pacific. We note that formation of thick BLs in
444 the October event is associated with a sudden relaxation of the winds between 26 and 27-October
445 (Figure 7b, c). There is no indication that the currents slowed or stopped as a result of this
446 (Figure 4). However, the disturbance in the wind forcing may have been enough to produce
447 submesoscale eddies (Thomas et al., 2008) and a growing set of convergences and divergences at
448 the surface (Figure 5) that were able to generate fronts and BLs during October 2017 (see also
449 Animation S1, 18-31-October-2017).

450 Tanguy et al. (2007) discuss the diversity of situations and causes responsible for the BLs
451 observed in the tropical Atlantic. Some instances of BLs arise in similar ways to those depicted
452 here in the ETP, on the fresh side of a mixed layer salinity front and at the front's base (see their
453 Figures 11c, e and f). As noted above, it has been hypothesized that BLs act to insulate the full
454 mixed layer from surface buoyancy flux and entrainment cooling from below (Godfrey and
455 Lindstrom, 1989; Vialard and Delecluse, 1998a) and concentrate heating into the upper part of
456 the mixed layer. If this is the case, then it follows that in the tropics, as these BLs are formed,
457 heating preferentially occurs on the fresh sides of submesoscale fronts. As the mixed layer is
458 heated in that region, the density contrast across the front is enhanced, along with the lifetime of
459 the front. This may be why these fronts can last for long periods of time, such as the one in the
460 Animation S2 which lasts more than two weeks, despite the fact that they are unstable. A
461 counterpoint to this is the fact that strong gradients in SST never develop in the two instances
462 where SSS fronts are studied, which we would have expected in the event of differential heating.

463 In this work, we have analyzed two very limited appearances of BLs, and attributed
464 certain characteristics to them. This is not to say that all, or even most, BLs in the ETP
465 necessarily follow this script. However, given the ubiquity of these features as seen in Animation
466 S1 and documented by KS20, there is no doubt the BLs introduce variance into the processes of
467 entrainment at the base of the mixed layer and the flux of heat and fresh water across the surface.
468 This variance itself may help to generate the submesoscale flows that create fronts (Thomas et al,
469 2008) and in turn work to increase variance in salinity, a positive feedback loop. This positive
470 feedback, acting on the large scale salinity field can perhaps lead to or accelerate the extension of
471 the surface salinity minimum that stretches across the tropical Pacific during the summer and fall
472 (Melnichenko et al., 2019).

473

474 **Acknowledgments and Data**

475 Color scales for all color figures were taken from the “cmocean” package (Thyng et al., 2016).

476 There are no known financial conflicts of interest on the parts of the authors of this paper, neither
477 are there any unstated affiliations among the authors that could be perceived as a conflict of
478 interest.

479 SPURS-2 central mooring data can be accessed here:

- 480 • <http://dx.doi.org/10.5067/SPUR2-MOOR1>

481 The authors express their appreciation to J. T. Farrar for providing this high quality dataset.

482 SPURS-2 uCTD data can be accessed here:

- 483 • <http://dx.doi.org/10.5067/SPUR2-UCTD0>

484 ROMS output can be accessed here:

- 485 • <http://dx.doi.org/10.15139/S3/UNJ8FX>

486 FB's work on SPURS-2 is supported by NASA grant NNX15AF72G, and by the Jet Propulsion
487 Laboratory through the Salinity Continuity Processing activity. SK is supported the Japan
488 Society for the Promotion of Science (JSPS) under its Overseas Research Fellowships program.
489 JS and SK are supported by NASA Grant Number 80NSSC18K1500. We wish to thank two
490 anonymous reviewers, who read the manuscript carefully and provided insightful comments.

491 **References**

- 492 Alory, G., C. Maes, T. Delcroix, N. Reul, and S. C. C. Illig (2012), Seasonal dynamics of sea
493 surface salinity off Panama: The far Eastern Pacific Fresh Pool, *Journal of Geophysical*
494 *Research*, 117(C4), C04028, doi:10.1029/2011JC007802.
- 495 Cronin, M. F., and M. J. McPhaden (2002), Barrier layer formation during westerly wind bursts,
496 *Journal of Geophysical Research: Oceans*, 107(C12), doi:10.1029/2001JC001171.
- 497 de Boyer Montegut, C., J. Mignot, A. Lazar, and S. Cravatte (2007), Control of Salinity on the
498 Mixed layer depth over the world ocean: 1. General Description, *Journal of Geophysical*
499 *Research*, C112, 6011, doi:10.1029/2006JC003953.
- 500 Fairall, C. W., E. F. Bradley, J. Hare, A. A. Grachev, and J. B. Edson (2003), Bulk
501 parameterization on air-sea fluxes: Updates and verification for the COARE algorithm,
502 *Journal of Climate*, 16, 571-591.
- 503 Farrar, J. T. (2019), SPURS-2 Central mooring CTD, surface flux and meteorological data for
504 the E. Tropical Pacific field campaign, NASA/JPL/PO.DAAC, Pasadena, CA,
505 doi:10.5067/SPUR2-MOOR1.
- 506 Farrar, J. T., and A. J. Plueddemann (2019), On the Factors Driving Upper-Ocean Salinity
507 Variability at the Western Edge of the Eastern Pacific Fresh Pool, *Oceanography*, 32,
508 doi:10.5670/oceanog.2019.209.
- 509 Fiedler, P. C., and L. D. Talley (2006), Hydrography of the eastern tropical Pacific: A review,
510 *Progress in Oceanography*, 69(2), 143-180, doi:10.1016/j.pocean.2006.03.008.
- 511 Godfrey, J. S., and E. J. Lindstrom (1989), The heat budget of the equatorial western Pacific
512 surface mixed layer, *Journal of Geophysical Research: Oceans*, 94(C6), 8007-8017,
513 doi:10.1029/JC094iC06p08007.
- 514 Good, S. A., M. J. Martin, and N. A. Rayner (2013), EN4: Quality controlled ocean temperature
515 and salinity profiles and monthly objective analyses with uncertainty estimates, *Journal*
516 *of Geophysical Research: Oceans*, 118(12), 6704-6716, doi:10.1002/2013JC009067.

- 517 Guimbard, S., N. Reul, B. Chapron, M. Umbert, and C. Maes (2017), Seasonal and interannual
518 variability of the Eastern Tropical Pacific Fresh Pool, *Journal of Geophysical Research:*
519 *Oceans*, 122(3), 1749-1771, doi:10.1002/2016JC012130.
- 520 Katsura, S., E. Oka, and K. Sato (2015), Formation Mechanism of Barrier Layer in the
521 Subtropical Pacific, *Journal of Physical Oceanography*, 45(11), 2790-2805,
522 doi:10.1175/JPO-D-15-0028.1.
- 523 Katsura, S., and J. Sprintall (2020), Seasonality and Formation of Barrier Layers and Associated
524 Temperature Inversions in the Eastern Tropical North Pacific, *Journal of Physical*
525 *Oceanography*, 50(3), 791-808, doi:10.1175/JPO-D-19-0194.1.
- 526 Katsura, S., J. Sprintall, and F. M. Bingham (2020), Upper Ocean Stratification in the Eastern
527 Pacific during the SPURS-2 Field Campaign, Preprint on essoar.org,
528 doi:10.1002/essoar.10504779.1.
- 529 Li, Z. (2020), SPURS-2 ROMS 1-Feb-2017 - 31-Jan-2018, doi:10.15139/S3/UNJ8FX.
- 530 Li, Z., F. M. Bingham, and P. P. Li (2019), Multiscale Simulation, Data Assimilation, and
531 Forecasting in Support of the SPURS-2 Field Campaign, *Oceanography*, 32,
532 doi:10.5670/oceanog.2019.221.
- 533 Li, Z., J. C. McWilliams, K. Ide, and J. D. Farrara (2015), A Multiscale Variational Data
534 Assimilation Scheme: Formulation and Illustration, *Monthly Weather Review*, 143(9),
535 3804-3822, doi:10.1175/MWR-D-14-00384.1.
- 536 Lindstrom, E., J., J. B. Edson, J. J. Schanze, and A. Y. Shcherbina (2019), SPURS-2: Salinity
537 Processes in the Upper-Ocean Regional Study 2 – The Eastern Equatorial Pacific
538 Experiment, *Oceanography*, 32, doi:10.5670/oceanog.2019.207.
- 539 Lukas, R., and E. Lindstrom (1991), The Mixed Layer of the Western Equatorial Pacific, *Journal*
540 *of Geophysical Research*, 96 (suppl.), 3343-3357, doi:10.1029/90JC01951.
- 541 Maes, C., J. Picaut, and S. Belamari (2002), Salinity barrier layer and onset of El Niño in a
542 Pacific coupled model, *Geophysical Research Letters*, 29(24), 59-51-59-54,
543 doi:10.1029/2002GL016029.
- 544 Maes, C., J. Picaut, and S. Belamari (2005), Importance of the Salinity Barrier Layer for the
545 Buildup of El Niño, *Journal of Climate*, 18(1), 104-118, doi:10.1175/JCLI-3214.1.
- 546 Melnichenko, O., P. Hacker, F. M. Bingham, and T. Lee (2019), Patterns of SSS Variability in
547 the Eastern Tropical Pacific: Intraseasonal to Interannual Timescales from Seven Years
548 of NASA Satellite Data, *Oceanography*, 32, doi:10.5670/oceanog.2019.208.
- 549 Pujol, M. I., Y. Faugère, G. Taburet, S. Dupuy, C. Pelloquin, M. Ablain, and N. Picot (2016),
550 DUACS DT2014: the new multi-mission altimeter data set reprocessed over 20 years,
551 *Ocean Sci.*, 12(5), 1067-1090, doi:10.5194/os-12-1067-2016.
- 552 Qu, T., Song, Y. T., and Maes, C. (2014), Sea surface salinity and barrier layer variability in the
553 equatorial Pacific as seen from Aquarius and Argo, *J. Geophys. Res. Oceans*, 119, 15–
554 29, doi:10.1002/2013JC009375.
- 555 Roemmich, D., M. Morris, W. R. Young, and J. R. Donguy (1994), Fresh Equatorial Jets,
556 *Journal of Physical Oceanography*, 24(3), 540-558, doi:10.1175/1520-
557 0485(1994)024<0540:FEJ>2.0.CO;2.

- 558 Rutledge, S.A., V. Chandrasekar, B. Fuchs, J. George, F. Junyent, P. Kennedy, and B. Dolan
559 (2019), Deployment of the SEA-POL C-band polarimetric radar to SPURS-2.
560 *Oceanography* 32(2):50–57, doi:10.5670/oceanog.2019.212.
- 561 Sato, K., T. Suga, and K. Hanawa (2004), Barrier layer in the North Pacific subtropical gyre,
562 *Geophysical Research Letters*, 31, 5301, doi:10.1029/2003GL018590.
- 563 Sato, K., T. Suga, and K. Hanawa (2006), Barrier layers in the subtropical gyres of the world's
564 oceans, *Geophysical Research Letters*, 33, L08603, doi:10.1029/2005GL025631.
- 565 Schanze, J. J., R. W. Schmitt, and L. L. Yu (2010), The global oceanic freshwater cycle: A state-
566 of-the-art quantification, *Journal of Marine Research*, 68(3-1), 569-595,
567 doi:10.1357/002224010794657164.
- 568 Shchepetkin, A. F. and J. C. McWilliams, J. C. (2011). Accurate Boussinesq oceanic modeling
569 with a practical, stiffened equation of state. *Ocean Modell.*, 38, 41–70.
- 570 Sprintall, J., and M. Tomczak (1992), Evidence for the Barrier Layer in the Surface layer of the
571 Tropics, *Jour. Geophys. Res. C Oceans*, 97, 7305-7316, doi:10.1029/92JC00407.
- 572 Sprintall, J. (2019a), SPURS-2 research vessel Underway CTD (uCTD) data for the E. Tropical
573 Pacific R/V Revelle cruises. Ver. 1.0. PO.DAAC, CA, USA. Dataset accessed 2020-07-
574 21 at doi:10.5067/SPUR2-UCTD0.
- 575 Sprintall, J. (2019b), Upper ocean salinity stratification during SPURS-2. *Oceanography*
576 32(2):40 - 41, doi:10.5670/oceanog.2019.210.
- 577 Tanguy, Y., S. Arnault, and P. Lattes (2010), Isothermal, mixed, and barrier layers in the
578 subtropical and tropical Atlantic Ocean during the ARAMIS experiment, *Deep Sea*
579 *Research Part I: Oceanographic Research Papers*, 57(4), 501-517,
580 doi:10.1016/j.dsr.2009.12.012.
- 581 Thomas, L. N., A. Tandon, and A. Mahadevan (2008) Sub-mesoscale processes and dynamics.
582 In M. W. Hecht, and H. Hasumi (Eds.), *Ocean Modeling in an Eddying Regime*,
583 *Geophysical Monograph Series*, Volume 177, American Geophysical Union, Washington
584 DC, pages 17-38.
- 585 Thompson, E.J., W.E. Asher, A.T. Jessup, and K. Drushka (2019), High-resolution rain maps
586 from an X-band marine radar and their use in understanding ocean freshening.
587 *Oceanography* 32(2):58–65, doi:10.5670/oceanog.2019.213.
- 588 Thyng, K. M., C. A. Greene, R. D. Hetland, H. M. Zimmerle, and S. F. DiMarco (2016), True
589 Colors of Oceanography: Guidelines for Effective and Accurate Colormap Selection,
590 *Oceanography*, 29(3), 9-13, doi:10.5670/oceanog.2016.66.
- 591 Veneziani, M., A. Griffa, Z. Garraffo, and J. A. Mensa (2014), Barrier Layers in the Tropical
592 South Atlantic: Mean Dynamics and Submesoscale Effects, *Journal of Physical*
593 *Oceanography*, 44(1), 265-288, doi:10.1175/JPO-D-13-064.1.
- 594 Vialard, J., and P. Delecluse (1998a), An OGCM Study for the TOGA Decade. Part I: Role of
595 Salinity in the Physics of the Western Pacific Fresh Pool, *Journal of Physical*
596 *Oceanography*, 28(6), 1071-1088, doi:10.1175/1520-
597 0485(1998)028<1071:AOSFTT>2.0.CO;2.

- 598 Vialard, J., and P. Delecluse (1998b), An OGCM Study for the TOGA Decade. Part II: Barrier-
599 layer Formation and Variability, *J. Phys. Oceanogr.*, 28(6), 1089-1106,
600 doi:10.1175/1520-0485(1998)028%3C1089:AOSFTT%3E2.0.CO;2.
- 601 Yu, L. (2015), Sea-surface salinity fronts and associated salinity-minimum zones in the tropical
602 ocean, *Journal of Geophysical Research Oceans*, 120, 4205–4225,
603 doi:10.1002/2015JC010790.
604